Crimson Publishers
Wings to the Research

Review Article

Thermodynamic Evaluation of the Corrosion Reactions in a Novel Superlight Mg-Li-Al-Y-Mn Alloy

Furong Cao[1,2]*, Huihui Shang[1,3], Chao Xiang[1], Nanpan Guo[1] and Shuting Kong[1]

[1]School of Materials Science and Engineering, Northeastern University, Shenyang 110819 China

[2]State Key Laboratory of Rolling and Automation, Northeastern University, Shenyang 110819 China

[3]AVIC Xi'an Aircraft Industry Group Company Ltd, China

ISSN: 2688-836X

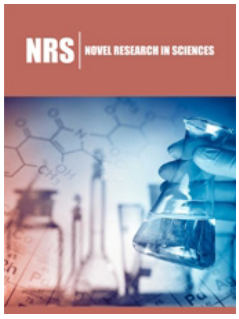

***Corresponding author:** Furong Cao, School of Materials Science and Engineering, State Key Laboratory of Rolling and Automation, Northeastern University, Shenyang, 110819, China

Submission: January 10, 2023
Published: January 13, 2023

Volume 13 - Issue 2

How to cite this article: Furong Cao*, Huihui Shang, Chao Xiang, Nanpan Guo, Shuting Kong. Thermodynamic Evaluation of the Corrosion Reactions in a Novel Superlight Mg-Li-Al-Y-Mn Alloy. Nov Res Sci. 13(2). NRS.000807. 2023.
DOI: 10.31031/NRS.2023.13.000807

Abstract

Magnesium-lithium alloy is the lightest alloy among non-toxic materials so far. It is used in aerospace, military, 3C electronics and automotive manufacturing. Poor corrosion performance is the main problem in the application of magnesium-lithium alloy. Therefore, this paper studies the corrosion resistance of Mg-Li-Al-Y-Mn alloy to seek ways to improve the corrosive performance of magnesium-lithium alloy. Multi-directional forging and asymmetric rolling are a new type of severe plastic deformation combined approach, which can effectively refine the grain. Therefore, multi-directional forging and asymmetric rolling are used to prepare Mg-9.55Li-2.92Al-0.027Y-0.026Mn alloy plate and study the alloy corrosion resistance by dynamic potential polarization curve and corrosion reaction thermodynamics. Compared to the dynamic potential polarization curve, it is found that the corrosion potential shifted from -1.5936v to -1.3687v, and the corrosion current density decreased from 1.1604×10^{-1}mA.cm^{-2} to 1.7689×10^{-4}mA.cm^{-2}, and the average corrosion rate decreased from 2.6515mm.a^{-1} to 4.0419×10^{-3}mm.a^{-1}, a difference of three orders of magnitude, so the corrosion resistance of the alloy is greatly improved. Thermodynamic evaluation of corrosion reaction shows that the reaction film formed by $Mg(OH)_2$(s), LiOH(s), Li_2CO_3(s), and $MgCO_3$(s) is beneficial to prevent further surface corrosion. This study shows that the corrosion resistance of the alloy is improved by multi-directional forging and asymmetric rolling, and thermodynamic evaluation provides basic data for the corrosion mechanism of the alloy.

Keywords: Mg-Li-Al alloy; Forging; Asymmetric rolling; Corrosion; Thermodynamics

Introduction

Due to ultra-low density, high specific stiffness, high specific strength, good damping properties and electromagnetic shielding properties, magnesium-lithium alloys are used in aerospace, military, 3C electronics and automotive manufacturing. Low strength and poor corrosion performance are the main problems puzzling the research of magnesium-lithium alloy. According to the literature research, the research on the corrosion and coating (protection) of magnesium-lithium alloy has become a hot topic in recent years, and people have developed various forms of coating, hoping to solve the corrosion resistance problem during the service of magnesium-lithium alloy [1-7]. However, although Esmaily et al. [8] mentioned the existence of a large number of corrosion chemical reactions in magnesium alloy corrosion, there is a lack of thermodynamic evaluation of the corrosion reactions in superlight magnesium-lithium alloys. Therefore, it is necessary to calculate the change of Gibbs free energy of chemical reaction from the perspective of thermodynamics, judge the role of reaction products, and deepen the understanding of corrosion mechanism. The severe plastic deformation methods, such as Equal Channel Corner Extrusion (ECAP), High Pressure Torsion (HPT), Friction Stir Machining (FSP), and Multi-Direction Forging (MDF) [9-12] are large strain deformation approaches which have been studied extensively in the past thirty years. In this paper, a method of MDF+AR (asymmetric rolling) combined

forming is proposed. It is expected that MDF+AR can be used to refine the grain, improve the mechanical properties and corrosion resistance of the alloy. Therefore, Mg-Li-Al-Y-Mn alloy plate was prepared in this paper, and the corrosion resistance of the alloy was studied by potentiodynamic polarization curve and corrosion thermodynamics. This report is expected to arouse interest in the thermodynamics of chemical reactions of magnesium lithium alloy corrosion researchers.

Experimental Process

Jackson flux-Argon gas protection method was used in the casting process of alloy ingot. The analytical composition of the present alloy was Mg-9.55Li-2.92Al-0.027Y-0.026Mn in wt.%. The ingot surface was milled and homogenized at 473K for 16 hours. The ingot was then cut into rectangular billets with a size of 40mm×32mm×22mm. Our previous MDF report was shown in Ref [13,14]. The cuboid billet was forged at 523K by changing the pressing direction continuously on a 300-ton press until it was subjected to 6 passes. The forged billets were then asynchronously rolled at 523K to 4mm thick with a reduction of 81.82% and further cold rolled to 2mm thick with a reduction of 50%. The speed ratio of asymmetric rolling was 1.2. In order to study the influence of processing deformation on the corrosion resistance of Mg-9.55Li-2.92Al-0.027Y-0.026Mn alloy, the dynamic potential polarization curves of as-cast and rolled alloy were measured. Potentiodynamic polarization curve was measured on CS series electrochemical workstation. Before the test, the samples were first wrapped with denture base polymer and denture base resin, and only the test surface was exposed. The test surface size of each sample was 10mm×10mm. Before the experiment, the samples were polished on 800#, 1500#, and 2000# abrasive papers in order to remove the oxide skin and other impurities on the surface. Rinsed with alcohol after grinding and immediately dried with air dryer.

After the sample was prepared, the dynamic potential polarization curve was tested. During the measurement, a three-electrode connection was adopted. The green current line (green jacket clip) was connected to the working electrode WE, the red current line (red jacket clip) was connected to the auxiliary electrode CE, and the yellow potential line (yellow jacket clip) was connected to the reference electrode RE. In this study, the alloy sample was used as the working electrode WE, the platinum electrode as the auxiliary electrode CE, the saturated calomel electrode as the reference electrode RE. The electrolyte was a solution of 3.5 wt.% analysis purity NaCl and distilled water. CorrTest software was used for measurement and data analysis during the experiment. The scanning range adopted in this study was the relative open circuit potential of -0.5V~1V, and the scanning rate was 5mV/s. Before the experiment, the sample was put into the 3.5wt. % NaCl solution for 5 min, and the test was carried out after the system was stabilized. In order to ensure the reliability of the experimental results, each group was tested three times.

Results and Discussion

Potentiodynamic polarization curves of as-cast and as-rolled alloys

The samples for potentiodynamic polarization curve experiment are from as-cast and as-rolled alloys, and the experimental results are shown in (Figure 1). As shown in Figure 1, both polarization curves consist of two parts: A cathode branch related to hydrogen evolution reduction reaction and an anode branch related to anode dissolution of the electrode. The two sides of the anode and cathode branches of the as-cast sample are obviously asymmetrical, and the current density in the anode region is relatively high. This is because the as-cast alloy has a negative potential, and hydrogen evolution reactions also occur in the anode region, forming a negative difference effect. However, the potential of the rolled alloy is positive, so it does not show obvious asymmetry. The cathodic corrosion potential Ecorr(V) and corrosion current density Jcorr(mA·cm^{-2}) can be fitted by the tafel extrapolation method in CorrTest software, and the corresponding average corrosion rate Pi(mm·a^{-1}) can be obtained from the formula Pi=22.85Jcorr, and the analytical values are shown in Table 1. It can be seen from Figure 1 and Table 1 that the as-cast and as-rolled alloy samples have different corrosion potential and cathode branch slope, respectively. Compared with the as-cast alloy, the corrosion potential of rolled alloy is moving from -1.5936V to -1.3687V. The corrosion current density decreases from 1.1604×10^{-1}mA·cm^{-2} to 1.7689×10^{-4} mA·cm^{-2}, and the average corrosion rate decreases from 2.6515mm·a^{-1} to 4.0419×10^{-3}mm·a^{-1}, a difference of three orders of magnitude, indicating that the corrosion resistance was greatly improved.

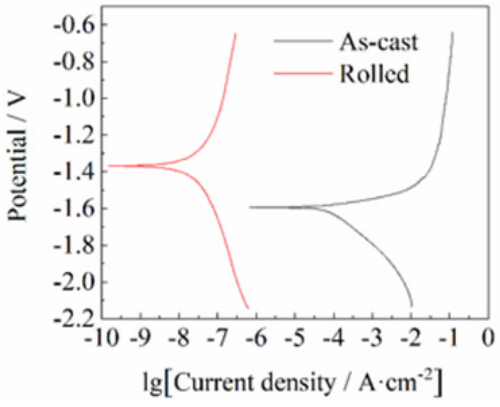

Figure 1: Potentiodynamic polarization curves of as-cast and as-rolled samples in 3.5 wt.% NaCl solution.

Table 1: Corrosion potential, corrosion current density and average corrosion rates of as-cast and rolled alloy samples.

Sample	E_{corr} (V)	J_{corr} (mA.cm^{-2})	b_c (mV)	P_i (mm.a$_{-1}$)
As-cast	-1.5936	1.1604×10^{-1}	245.07	2.6515
As-rolled	-1.3687	1.7689×10^{-4}	3837.6	4.0419×10^{-3}

Thermodynamic evaluation of corrosion reactions

The cathode reaction and the anode reaction equations [15,16] are shown in (1) to (9).

Cathodic reaction

$2H_2O+2e\text{-}\rightarrow H_2+2OH^-$ (1)

Anodic reactions and corrosion products

$Mg\rightarrow Mg^{2}++2e-$ (2)

$Li\rightarrow Li++e-$ (3)

$Mg^{2}++2OH-\rightarrow Mg(OH)^{2}$ (4)

$Li++OH-\rightarrow LiOH$ (5)

$2Mg+O_2\rightarrow 2MgO$ (6)

$4Li+O_2\rightarrow 2Li_2O$ (7)

$MgO+CO_2\rightarrow MgCO_3$ (8)

$Li_2O+CO_2\rightarrow Li_2CO_3$ (9)

The thermodynamic formula is as follows:

$$\Delta_r H_m^{\theta} = \sum \nu_B \Delta_f H_m^{\theta}(B) \quad (10)$$

$$\Delta_r S_m^{\theta} = \sum \nu_B S_m^{\theta}(B) \quad (11)$$

$$\Delta_r G_m^{\theta} = \Delta_r H_m^{\theta} - T\Delta_r S_m^{\theta} = -RT\ln K^{\theta} \quad (12)$$

$$K^{\theta} = \frac{e^{-\Delta_r G_m \theta}}{RT} \quad (13)$$

Where: v_B is the coefficient in the equation; ΔfHm^{θ} is the standard molar enthalpy of formation, in kJ·mol^{-1}; Sm^{θ} is the standard molar entropy, unit: J·K^{-1}.mol^{-1}; ΔrHm^{θ} is the standard molar enthalpy of reaction, in kJ·mol-1; ΔrSm^{θ} is the standard molar entropy change, and the unit is J·K^{-1}·mol^{-1}; R is the molar gas constant, 8.314J·K^{-1}·mol^{-1}; T is the absolute temperature, 298K in this study; ΔrGm^{θ} is the standard Gibbs function variation, in kJ.mol^{-1}; K^{θ} is the standard equilibrium constant.

The thermodynamic parameters of each chemical reaction can be calculated according to formula (10)~(13) [15,16], and the specific results are shown in Tables 2-4 [17,18]. Among them, the Gibbs function variation of each reaction is less than 0, which means that each reaction can proceed spontaneously. The value of the standard equilibrium constant represents the degree of reaction progress. Under a certain temperature, the greater the value of the standard equilibrium constant, the greater the degree of reaction is positive. According to the analysis of chemical valence change before and after the reaction, Mg becomes +2 from 0, Li from 0 to +1, H from +1 to -1, and O from 0 to -2. Therefore, all the chemical reactions here are REDOX reactions, in which Mg and Li lose electrons and become reducing agents, H_2O and O_2 gain electrons. It is an oxidant. According to the sequence of REDOX reaction, the same reducing agent is added into several oxidant solutions, and the oxidizing agent with strong oxidizing ability is reduced first. Since O_2 is more oxidizing than H_2O, when Mg-Li alloy corrodes, Mg and Li react with O_2 first to form MgO and Li_2O, and then react with H_2O to form $Mg(OH)_2$ and LiOH. It was reported [19] that Mg-Li alloy corrodes in the atmosphere and forms a multi-component oxide film on its surface, which contains four layers. From the inside (near the matrix) to the outside (near the atmosphere) are Li_2O+MgO+Mg+Li, LiOH+MgO+$Mg(OH)_2$+Li_2O+Mg, Li_2O+$Mg(OH)_2$+MgO and Li_2O+$Mg(OH)_2$, respectively. It can be seen that MgO and Li_2O+$Mg(OH)_2$ are formed during the formation of the oxide film. $Mg(OH)_2$ and LiOH were regenerated. In terms of the equilibrium constant, the degree of $Mg(OH)_2$ formation was much greater than that of LiOH formation, which was consistent with the reaction order speculated in this paper. At the same time, due to the presence of atmospheric CO_2, Li_2O reacts with CO_2 to produce Li_2CO_3, and MgO reacts with CO_2 to produce $MgCO_3$. As per the equilibrium constant, the degree of Li_2CO_3 generation is far greater than the degree of $MgCO_3$ generation, indicating that the generated Li_2CO_3 is more stable than $MgCO_3$.

Table 2: Thermodynamic data obtained from the literature [17,18].

Chemical Compound	Temperature T(K)	Standard Molar Enthalpy $y\Delta_f H_m^{\theta}$ (kJ·mol^{-1})	Standard Molar Entropy S_m^{θ} (J·K^{-1}·mol^{-1})
Mg(s)	298	0	32.68
Li(s)	298	0	29.08
O_2(g)	298	0	205.04
H_2O(g)	298	-241.81	188.72
H_2(g)	298	0	130.58
MgO (s)	298	-601.24	26.94
Li_2O(s)	298	-598.73	37.89
$Mg(OH)_2$(s)	298	-924.66	63.18
LiOH(s)	298	-484.67	42.68
CO_2(g)	298	-393.51	213.66
Li_2CO_3(s)	298	-1215.87	90.17
$MgCO_3$(s)	298	-1111.69	65.86

Table 3: Standard molar reaction enthalpy change $\Delta_r H_m^\theta$ and standard molar entropy change $\Delta_r S_m^\theta$ of each chemical reaction.

Chemical Reactions	Standard Molar Enthalpy Change $\Delta_r H_m^\theta$ (kJ.mol^{-1})	Standard Molar Entropy Change $\Delta_r S_m^\theta$ (J.K^{-1}.mol^{-1})
$Mg(s)+1/2O_2(g)=MgO(s)$	-601.24	-108.26
$2Li(s)+1/2O_2(g)=Li_2O(s)$	-598.73	-122.79
$Mg(s)+2H_2O(g)=Mg(OH)_2(s)+H_2(g)$	-441.04	-216.36
$Li(s)+H_2O(g)=LiOH(s)+1/2H_2(g)$	-242.86	-109.83
$MgO(s)+CO_2(g)\rightarrow MgCO_3(s)$	-116.94	-174.74
$Li_2O(s)+CO_2(g)\rightarrow Li_2CO_3(s)$	-223.63	-161.38

Table 4: Standard Gibbs function change $\Delta_r G_m^\theta$ and standard equilibrium constant K^θ of each chemical reaction.

Chemical Reactions	Standard Gibbs Function Change $\Delta_r G_m^\theta$ (kJ.mol^{-1})	Standard Equilibrium Constant K^θ
$Mg(s)+1/2O_2(g)=MgO(s)$	-568.98	5.45E+99
$2Li(s)+1/2O_2(g)=Li_2O(s)$	-562.14	3.45E+98
$Mg(s)+2H_2O(g)=Mg(OH)_2(s)+H_2(g)$	-376.56	1.02E+66
$Li(s)+H_2O(g)=LiOH(s)+1/2H_2(g)$	-210.13	6.82E+36
$MgO(s)+CO_2(g)\rightarrow MgCO_3(s)$	-64.87	2.35E+11
$Li_2O(s)+CO_2(g)\rightarrow Li_2CO_3(s)$	-175.54	5.89E+30

The products of $Mg(OH)_2(s)$, LiOH(s), $MgCO_3$ and Li_2CO_3 are stable films, which prevent further corrosion. Li et al. [20] studied the corrosion and electrochemical behavior of Mg-4Li(α), Mg-7.5Li (α+β) and Mg-14Li (β) alloys and investigated the effect of crystal structure on the corrosion resistance of Mg-Li binary system. The corrosion resistance was tested in 0.1M NaCl solution, and the corrosion rates of the three alloys were found to be Mg-7.5Li >Mg-4Li>Mg-14Li from high to low. The results show that the corrosion resistance and electrochemical behavior of Mg-Li alloy vary with the composition and crystal structure. The corrosion resistance of α+β biphase Mg-Li alloy is worse than that of single-phase Mg-Li alloy. Moreover, the β-Li phase of BCC structure contributes to the formation of protective surface films. The single phase β-Li solid solution Mg-Li alloy with BCC structure has higher corrosion resistance than the single phase α-Mg solid solution Mg-Li alloy with HCP structure. Zhao et al. [21] studied the corrosion behavior of α-Mg based Mg-4Li- (3AlSi) alloy and β-Li base Mg-12Li-(3AlSi) alloy and found that the corrosion resistance of α-Mg is better than that of β-Li, and the corrosion is related to the phase composition. Despite the differences in the above-mentioned research results, the existence of Li_2CO_3 and $MgCO_3$ corrosion films produced by thermodynamic evaluation prevents further corrosion, which is the reason for the increase in corrosion resistance of β-Li phase alloys. Dobkawska et al. [22] recently found that the corrosion resistance of α+β biphasic Mg-Li alloys is reduced due to the action of micro-galvanic couples.

Sun et al. [23] studied the microstructure and corrosion behavior of three homogenized LAZ532-0.20Zr, LAZ832-0.20Zr and LAZ1132-0.20Zr alloys with α, α+β and β as the matrix, respectively, and found that the homogenized LAZ832-0.20Zr with α+β as the matrix had the best corrosion resistance. This indicates that due to the different processing history, the corrosion experiment results of different authors are different. At present, there are two views on the effect of grain refinement on corrosion resistance: opposing and supporting. The opposing view is that even though the grain size of the biphase alloy is finer, the corrosion resistance of the alloy is reduced due to the action of the micro-galvanic couple. Our research results support the view that grain refinement improves corrosion resistance. This is because the severe plastic deformation of MDF+AR results in grain refinement and second phase breakage, which increase the homogeneity of the structure, weaken the micro-galvanic couple effect and improve the corrosion resistance.

He et al. [24] studied the effects of Li, Al and Y elements on the microstructure and corrosion behavior of Mg-Li-Al-(Y) alloy, and the results showed that the alloy elements affecting the corrosion behavior of Mg-Li-Al-(Y) alloy were Al>Li>Y from strong to weak. In addition, it is found that Mg-10Li-3Al-0.6Y alloy has better corrosion resistance. The main reason is that the α-Mg phase of the alloy has uniform microstructure, high area fraction and uniform distribution, which acts as the corrosion barrier to inhibit the severe local dissolution of β-Li matrix. According to the XRD patterns of the as-cast and as-rolled state [25], compared with the as-cast state, the intensity and number of the characteristic peaks of α-Mg phase and Li_2MgAl phase in the rolled state are slightly decreased, while the intensity of the characteristic peaks of β-Li phase is significantly increased, which indicates that the content of α-Mg and Li_2MgAl phase is decreased, while the content of β-Li phase is significantly increased. The process may promote the transformation of α-Mg into β-Li phase. On the one hand, the increase of β-Li phase content contributes to the formation of surface protective film, on the other hand, the micro-galvanic coupling between phases is greatly reduced. Therefore, since the rolled grain size of Mg-9.55Li-2.92Al-

0.027Y-0.026Mn alloy is finer to 1.9μm because of the dominance of the β-Li phase, the corrosion resistance of rolled state is greatly improved compared with that of as-cast state.

Conclusion

Mg-9.55Li-2.92Al-0.027Y-0.026Mn alloy plate was prepared by multidirectional forging and rolling. The corrosion resistance of the alloy was studied by potentiodynamic polarization curve and corrosion thermodynamics.

i. The potentiodynamic polarization curve showed that compared with the cast state, the corrosion potential of rolled state moved from -1.5936V to -1.3687V, and the corrosion current density decreased from 1.1604×10^{-1}mA.cm^{-2} to 1.7689×10^{-4}mA.cm^{-2}. The average corrosion rate decreases from 2.6515mm.a^{-1} to 4.0419×10^{-3}mm.a^{-1}, a difference of three orders of magnitude, showing that the corrosion resistance is greatly improved.

ii. Thermodynamic evaluation of corrosion reaction shows that the reaction film formed by $Mg(OH)_2$(s), LiOH(s), Li_2CO_3(s) and $MgCO_3$(s) is beneficial to prevent further corrosion on the surface.

References

1. Dobkowska A, Koralnik KM, Adamczyk-Cieslak B, Kuc D, Chromiński W, et al. (2022) The effect of extrusion ratio on the corrosion resistance of ultrafine-grained Mg-4Li-3Al-Zn alloy deformed using extrusion with a forward-backward oscillating die. J Mater Eng Perform 31: 8932-8939.
2. Zheng XY, Lai HS, Zhao ZL (2021) Preparation of iron Tetradecanoate coating on the surface of Mg-Li alloy and its corrosion resistance. Int J Electrochem Sci 16: 1-8.
3. Dong LJ, Liu X, Liang JX, Li CQ, Dong Y, et al. (2021) Corrosion behavior of a eutectic Mg-8Li alloy in NaCl solution. Electrochem Commu 129.
4. Yu C, Cui LY, Zhou YF, Han ZZ, Chen XB, et al. (2018) Self-degradation of micro-arc oxidation/chitosan composite coating on Mg-4Li-1Ca alloy. Surf Coat Technol 344: 1-11.
5. Wan SM, Cui XF, Jin QW, Ma JJ, Wen X, et al. (2022) Microstructure and properties of cold sprayed aluminum bronze coating on MBLS10A-200 magnesium-lithium alloy. Mater Chem Phys 281.
6. Li CQ, Deng BB, Dong LJ, Shi BQ, Dong Y, et al. (2022) Effect of Zn addition on the corrosion behaviours of as-cast BCC Mg-11Li based alloys in NaCl solution. Mater Des 221.
7. Ma XC, Jin SY, Wu RZ, Ji Q, Hou LG, et al. (2022) Influence alloying elements of Al and Y in Mg-Li alloy on the corrosion behavior and wear resistance of microarc oxidation coatings. Surf Coat Technol 432.
8. Esmaily M, Svensson JE, Fajardo S, Birbilis N, Frankel GS, et al. (2017) Fundamentals and advances in magnesium alloy corrosion. Prog Mater Sci 89: 92-193.
9. Valiev RZ, Straumal B, Langdon TG (2022) Using severe plastic deformation to produce nanostructured materials with superior properties. Annu Rev Mater Res 52: 357-382.
10. Langdon TG (2013) Twenty-five years of ultrafine-grained materials: Achieving exceptional properties through grain refinement. Acta Mater 61(19): 7035-7059.
11. Mishra RS, Ma ZY (2005) Friction stir welding and processing. Mater Sci Eng R 50(1-2): 1-78.
12. Cao FR, Zhang J, Ding X, Xue GQ, Liu SY, et al. (2019) Mechanical properties and microstructural evolution in a superlight Mg-6.4Li-3.6Zn-0.37Al-0.36Y alloy processed by multidirectional forging and rolling. Mater Sci Eng A 760: 377-393.
13. Cao F, Xue G, Xu G (2017) Superplasticity of a dual-phase-dominated Mg-Li-Al-Zn-Sr alloy processed by multidirectional forging and rolling. Mater Sci Eng A 704: 360-374.
14. Cao F, Sun C, Liu S, Liang J, Liu R, et al. (2022) Microstructures, hot tensile deformation behavior and constitutive modeling in a superlight Mg-2.76Li-3Al-2.6Zn-0.39Y alloy. J Alloys Compd 896.
15. Wang B, Luan J, XU D, Sun J, Li C, et al. (2019) Research progress on the corrosion behavior of magnesium-lithium-based alloys: A review. Acta Metall Sin 32: 1-9.
16. Ma X, Jin S, Wu R, Wang J, Wang G, et al. (2021) Corrosion behavior of Mg–Li alloys: A review. Trans Nonferrous Met Soc China 31(11): 3228-3254.
17. Shi JY, Lv BT, Dong YY (2014) Concise physical chemistry. Science Press, China, pp. 1-6
18. Liang YJ, Che YC (1993) Handbook of inorganic materials thermodynamics. Northeastern University Press, China, pp. 1-8.
19. Gao XH, Li YF, Zhu JJ (2017) Corrosion mechanism and surface protection method for magnesium-lithium alloy. Chem Ind Eng Prog 36: 3373-3379.
20. Li CQ, Xu DK, Chen XB, Wang BJ, Wu RZ, et al. (2018) Composition and microstructure dependent corrosion behaviour of Mg-Li alloys. Electrochimica Acta 260: 55-64.
21. Zhao ZL, Liu YD, Zhong YF, Chen XH, Zhang ZQ (2018) Corrosion resistance of as-rolled Mg-Li-AlSi alloys. Int J Electrochem Sci 13: 4338-4349.
22. Dobkowska A, Cieslak BA, Koralnik M, Chrominski W, Kubasek J, et al. (2022) Corrosion behavior of fine-grained Mg-7.5Li-3Al-1Zn fabricated by extrusion with a forward-backward rotating die (KoBo). J Mag Alloys 10(3): 811-820.
23. Sun Y, Wang R, Peng C, Wang X (2020) Microstructure and corrosion behavior of as-homogenized Mg-xLi-3Al-2Zn-0.2Zr alloys (x=5,8,11 wt%). Mater Charact 159.
24. He Y, Peng C, Feng Y, Wang R, Zhong J (2020) Effects of alloying elements on the microstructure and corrosion behavior of Mg-Li-Al-Y alloys. J Alloys Compd 834.
25. Cao F, Shang H, Guo N, Kong S, Liu R (2022) High strain rate quasi-superplasticity behavior in an ultralight Mg-9.55Li-2.92Al-0.027Y-0.026Mn alloy fabricated by multidirectional forging and asymmetrical rolling. Mater 15: 1-15.